

Geometrical Properties of Two-Dimensional Interacting Self-Avoiding Walks at the θ -Point

Sergio Caracciolo

Dipartimento di Fisica and INFN — Sezione di Milano I
Università degli Studi di Milano
Via Celoria 16, I-20133 Milano, Italy
 e-mail: `Sergio.Caracciolo@mi.infn.it`

Marco Gherardi

Dipartimento di Fisica and INFN — Sezione di Milano I
Università degli Studi di Milano
Via Celoria 16, I-20133 Milano, Italy
 e-mail: `Marco.Gherardi@mi.infn.it`

Mauro Papinutto

Laboratoire de Physique Subatomique et de Cosmologie,
UJF/CNRS-IN2P3/INPG, 53 rue des Martyrs, F-38026 Grenoble, France
 e-mail: `Mauro.Papinutto@lpsc.in2p3.fr`

Andrea Pelissetto

Dipartimento di Fisica and INFN — Sezione di Roma I
Università degli Studi di Roma “La Sapienza”
P.le A.Moro 2, I-00185 Roma, Italy
 e-mail: `Andrea.Pelissetto@roma1.infn.it`

February 16, 2022

Abstract

We perform a Monte Carlo simulation of two-dimensional N -step interacting self-avoiding walks at the θ point, with lengths up to $N = 3200$. We compute the critical exponents, verifying the Coulomb-gas predictions, the θ -point temperature $T_\theta = 1.4986(11)$, and several invariant size ratios. Then, we focus on the geometrical features of the walks, computing the instantaneous shape ratios, the average asphericity, and the end-to-end distribution function. For the latter quantity, we verify in detail the theoretical predictions for its small- and large-distance behavior.

1 Introduction

Self-avoiding walks (SAWs) have been extensively studied during the years. They have a rich mathematical structure and represent one of the simplest models of critical behavior. Moreover, they are also relevant for the understanding of the universal features of large-molecular-weight macromolecules in solution [1–8]. Indeed, the study of the asymptotic behavior of long SAWs (and also of walks with different architecture, like self-avoiding rings or stars) allows one to obtain predictions for several structural and thermodynamical properties — for instance critical exponents, structure factors, osmotic pressure, etc. — of polymers both in dilute and in semidilute good-solvent solutions in the limit of infinite degree of polymerization. These predictions are in good agreement with the (usually much less precise) experimental results. By adding an attractive interaction SAWs also allow us to study the critical transition (θ -point) between good-solvent and poor-solvent behavior [5–8]. The phase diagram of interacting SAWs is well-known. Above the θ -temperature T_θ , the large- N behavior is temperature-independent and in the same universality class as that observed for athermal SAWs, which correspond to the case $T = \infty$. On the other hand, for $T < T_\theta$ typical walks are compact: this is the so-called collapsed or poor-solvent regime. At the θ temperature, interacting SAWs show a quite interesting tricritical behavior. The two-dimensional case has been extensively studied by Coulomb-gas techniques and conformal field theory (CFT). They have provided exact predictions for the critical exponents [9], which have been confirmed by several high-precision numerical studies [10–22]. Also the collapsed phase has been discussed in detail [23–27], including the crossover behavior close to the θ point [28].

In this paper we perform a Monte Carlo (MC) simulation of two-dimensional interacting SAWs close to the θ point, with the purpose of determining some geometrical features of the walks. In particular, we shall focus on the instantaneous shape of the walks and on the end-to-end distribution function (EEDF). As is well known, walks are not instantaneously spherical. Their shape is usually characterized by considering combinations of the eigenvalues of the gyration tensor. One of them, the mean asphericity, is an essential ingredient in theoretical studies of the hydrodynamic behavior of dilute polymer solutions [29–31]. The EEDF has been extensively studied in three-dimensions, because of its theoretical interest [32–44]. Under the mapping of SAWs onto the $n \rightarrow 0$ σ model (or $\lambda\phi^4$ theory), it corresponds to the spin-spin correlation function, which is the basic object of field-theoretical calculations. Moreover, it can be also accessed experimentally, by performing neutron-scattering experiments on solutions of end-marked polymers [7].

In this paper we will obtain a high-precision determination of the EEDF, which will be compared with several predictions obtained by using the standard mapping onto the $n = 0$ spin model and with phenomenological expressions that have been shown to be quite accurate in three dimensions. As for the shape of the walks, we will determine the average asphericity, comparing it with results obtained in the good-solvent regime [45, 46] and for noninteracting random walks [47].

The paper is organized as follows. In Sec. 2 we define the interacting SAWs and some basic quantities. In Sec. 3 we use our MC results to determine the θ temperature

and verify the theoretical predictions for the critical exponents. In Sec. 4 we study the walk shape and in Sec. 5 the EEDF. Finally, in Sec. 6 we summarize our conclusions.

2 Model and definitions

In this paper we consider self-avoiding walks (SAWs) on a two-dimensional square lattice. An N -step SAW ω is a set of $N + 1$ lattice sites $\omega_0 = 0, \omega_1, \dots, \omega_N$, such that ω_i and ω_{i+1} are lattice nearest neighbors. For each walk, we define the energy \mathcal{E} as follows:

$$\mathcal{E} \equiv - \sum_{i=0}^{N-3} \sum_{j=i+3}^N c_{ij}, \quad (2.1)$$

where

$$c_{ij} \equiv \begin{cases} 1 & \text{if } |\omega_i - \omega_j| = 1; \\ 0 & \text{otherwise.} \end{cases} \quad (2.2)$$

Essentially, \mathcal{E} is the number of nearest-neighbor contacts without considering the trivial contacts between subsequent monomers.

We consider the ensemble of N -step walks with partition function

$$Z_N = \sum_{\{\omega\}} e^{-\beta \mathcal{E}}, \quad (2.3)$$

where β is the inverse temperature and the sum is extended over all N -step walks. We will study the behavior close to the θ temperature β_θ . For the model we consider, the best present-day estimates of β_θ on the square lattice are reported in Table 1.

We consider three different observables that measure the size of the walk:

- the square end-to-end distance

$$R_e^2 \equiv (\omega_N - \omega_0)^2; \quad (2.4)$$

- the square radius of gyration

$$R_g^2 \equiv \frac{1}{N+1} \sum_{i=0}^N \left(\omega_i - \frac{1}{N+1} \sum_{k=0}^N \omega_k \right)^2 = \frac{1}{2(N+1)^2} \sum_{i,j=0}^N (\omega_i - \omega_j)^2; \quad (2.5)$$

- the square monomer distance from an endpoint

$$R_m^2 \equiv \frac{1}{N+1} \sum_{i=0}^N (\omega_i - \omega_0)^2. \quad (2.6)$$

Correspondingly, we define the universal ratios

$$A_N \equiv \frac{\langle R_g^2 \rangle_N}{\langle R_e^2 \rangle_N}, \quad B_N \equiv \frac{\langle R_m^2 \rangle_N}{\langle R_e^2 \rangle_N}, \quad C_N \equiv \frac{\langle R_g^2 \rangle_N}{\langle R_m^2 \rangle_N}, \quad (2.7)$$

	year	method	β_θ
Ref. [10]	1987	EE	0.75
Ref. [11]	1988	MC	0.65(3)
Ref. [12]	1990	EE	0.67(4)
Ref. [13]	1990	MC	0.658(4)
Ref. [14]	1992	EE	0.657(16)
Ref. [15]	1993	MC	0.658(4)
Ref. [16]	1994	EE	0.660(5)
Ref. [17]	1995	MC	0.665(2)
Ref. [18]	1996	MC	0.664, 0.666
Ref. [48]	1997	MC	0.667(1)
Ref. [49]	2009	MC	0.664(8)
this work	2010	MC	0.6673(5)

Table 1: Estimates of β_θ on the square lattice. EE stands for exact enumeration, MC for Monte Carlo.

and the combination (the exponents γ_θ and ν_θ are defined below)

$$F_N \equiv \left(2 + \frac{2}{\gamma_\theta + 2\nu_\theta}\right) A_N - 2B_N + \frac{1}{2} = \frac{23}{8}A_N - 2B_N + \frac{1}{2}. \quad (2.8)$$

For two-dimensional non-interacting SAWs it has been proved [50, 51] that the corresponding F_N (with the appropriate exponents γ and ν) vanishes in the limit $N \rightarrow \infty$. It has been conjectured and verified numerically [16] that $F_\infty = 0$ also at the θ point.

In a neighborhood of β_θ the radii have a scaling behavior of the form

$$\langle R^2 \rangle_N = N^{2\nu_\theta} f(x) \quad x \equiv N^\phi (\beta - \beta_\theta), \quad (2.9)$$

with $f(0) \neq 0$. More precisely, this scaling form is valid for $\beta \rightarrow \beta_\theta$, $N \rightarrow \infty$ at fixed x . In two dimensions, CFT and Coulomb-gas techniques allow us to compute the universal exponents ϕ and ν_θ . They are given by [9]

$$\nu_\theta = \frac{4}{7}, \quad \phi = \frac{3}{7}. \quad (2.10)$$

The crossover exponent ϕ can be measured directly at $\beta = \beta_\theta$ by considering the specific heat h_N , which scales as

$$h_N \equiv \frac{1}{N} (\langle \mathcal{E}^2 \rangle_N - \langle \mathcal{E} \rangle_N^2) \sim N^{2\phi-1}, \quad (2.11)$$

or the temperature dependence of the radii,

$$D_N \equiv -\frac{1}{\langle R^2 \rangle_N} \frac{d\langle R^2 \rangle_N}{d\beta} = \langle \mathcal{E} \rangle_N - \frac{\langle R^2 \mathcal{E} \rangle_N}{\langle R^2 \rangle_N} \sim N^\phi. \quad (2.12)$$

N	$\langle R_g^2 \rangle_N$	$\langle R_e^2 \rangle_N$	$\langle R_m^2 \rangle_N$	$\langle \mathcal{E} \rangle_N$	h_N
100	43.438(8)	241.87(7)	123.02(3)	46.304(2)	68.10(2)
800	472.72(30)	2604(3)	1332(1)	429.712(26)	909.53(60)
1600	1050.19(37)	5784(3)	2957(1)	877.717(21)	2034.49(68)
3200	2338.7(1.5)	12895(13)	6584(5)	1780.259(53)	4460.2(2.5)

N	A_N	B_N	C_N	D_N	F_N
100	0.179592(61)	0.50863(18)	0.35309(97)	2.2793(15)	-0.0009(4)
800	0.18152(22)	0.51139(64)	0.35496(35)	6.826(15)	-0.0009(14)
1600	0.18156(12)	0.51123(35)	0.35514(19)	9.54(1)	-0.0005(8)
3200	0.18137(21)	0.51060(63)	0.35521(35)	13.170(29)	0.0002(14)

Table 2: Estimates of $\langle R_g^2 \rangle_N$, $\langle R_e^2 \rangle_N$, $\langle R_m^2 \rangle_N$, $\langle \mathcal{E} \rangle_N$, h_N , A_N , B_N , C_N , D_N , and F_N .

In the analysis of the end-to-end distribution function we will also consider the exponent γ_θ , which controls the large- N behavior of the partition function at the θ temperature,

$$Z_N \sim \mu^N N^{\gamma_\theta - 1}, \quad (2.13)$$

where μ is a lattice- and model-dependent constant. The exponent γ_θ is universal; CFT and Coulomb-gas calculations predict [9] $\gamma_\theta = 8/7$.

3 Determination of the critical exponents

We performed a MC simulation using the extended reptation algorithm discussed in detail in Refs. [52, 53]. We fixed $\beta = 0.665$, which is the estimate of β_θ presented in Ref. [17], and performed runs for $N = 100, 800, 1600, 3200$. Some results are reported in Table 2. Since β_θ is not exactly known, we also computed several quantities for $\beta = 0.665 - 0.0005n$, $n = 1, 2, 3, 4$, using the standard reweighting method.

In order to determine ν_θ we perform fits of the radii. If we fit all data at $\beta_\theta = 0.665$ to $aN^{2\nu_\theta}$ we obtain $\nu_\theta \approx 0.573$, while, if we discard the results corresponding to $N = 100$, we obtain $\nu_\theta \approx 0.577$. These estimates are close to the theoretical prediction $\nu_\theta = 4/7 \approx 0.5714\dots$. The slight discrepancy is probably due to the fact that $\beta = 0.665$ is slightly smaller than the θ -value β_θ , so that we are seeing the beginning of the crossover towards the good-solvent value $\nu = 3/4$. A better analysis consists in fitting the data at $\beta = 0.665$ and the reweighted data to Eq. (2.9). Since x is small for our data, assuming that the function $f(x)$ is regular at $x = 0$, we can expand it in powers of x . At first order we obtain the scaling form

$$\langle R^2 \rangle_N = aN^{2\nu_\theta} + bN^{2\nu_\theta + \phi}(\beta - \beta_\theta), \quad (3.1)$$

valid for $x \equiv N^\phi(\beta - \beta_\theta) \ll 1$. We first perform fits taking a , b , ν_θ , ϕ , and β_θ as free parameters. The results are reported in Table 3, as a function of N_{\min} , the minimum

	N_{\min}	ν	ϕ	β_θ	β_θ (f.exp.)
R_g	100	0.5720(2)	0.480(4)	0.6669(1)	0.6675(1)
	800	0.5721(2)	0.480(5)	0.6669(1)	0.6675(1)
R_e	100	0.5678(3)	0.480(5)	0.6677(1)	0.6670(1)
	800	0.5683(3)	0.480(5)	0.6676(1)	0.6670(1)
R_m	100	0.5706(3)	0.478(6)	0.6672(1)	0.6671(1)
	800	0.5711(3)	0.478(5)	0.6670(1)	0.6671(1)

Table 3: Estimates of the exponents and of β_θ obtained by fitting the reweighted data to Eq. (3.1). The critical value β_θ in the rightmost column [β_θ (f.exp.)] is obtained by fixing the theoretical values for the exponents, i.e., by fitting the data to $\langle R^2 \rangle_N = aN^{8/7} + bN^{11/7}(\beta - \beta_\theta)$.

length allowed in the fits. The results obtained in the analysis of the three ratios are reasonably close and indicate

$$\nu_\theta = 0.570(2), \quad (3.2)$$

$$\phi = 0.479(6), \quad (3.3)$$

$$\beta_\theta = 0.6673(5), \quad (3.4)$$

$$T_\theta = 1/\beta_\theta = 1.4986(11). \quad (3.5)$$

These estimates are the average of all fits and the reported error is such to include all results and the corresponding errors. The exponent ν_θ is in good agreement with the Coulomb-gas prediction $\nu_\theta = 4/7 \approx 0.571$. On the other hand, the exponent ϕ is significantly larger than $\phi = 3/7 \approx 0.429$. This may be due to neglected scaling corrections and/or to the neglected terms in the expansion of the function $f(x)$, although, we must admit, we have no evidence of corrections in our results, which are stable with respect to N_{\min} and to the observable considered.

The estimate of β_θ is in good agreement with the most recent one obtained in Ref. [48], in which much longer walks were used. The fit in which we assume the theoretical values of the exponents gives estimates of β_θ that have a significantly smaller statistical error, see Table 3. However, note that we neglect here scaling corrections which can — and probably do, given the observed discrepancy for the exponent ϕ — give rise to systematic deviations which are larger than the tiny statistical errors. Hence, we shall keep the conservative estimate (3.4).

In order to obtain independent estimates of the crossover exponent, we also analyze D_N and h_N . By fitting the MC data we obtain $\phi = 0.450(4)$ (from h_N) and $\phi = 0.436(5)$ (from D_N). They differ significantly from the estimate (3.3), and thus provide evidence that the apparent stability observed in the fits of the radii and, therefore, the relatively small error, should not be trusted. The estimate from the analysis of h_N and D_N are in better agreement with the theoretical value than the estimate

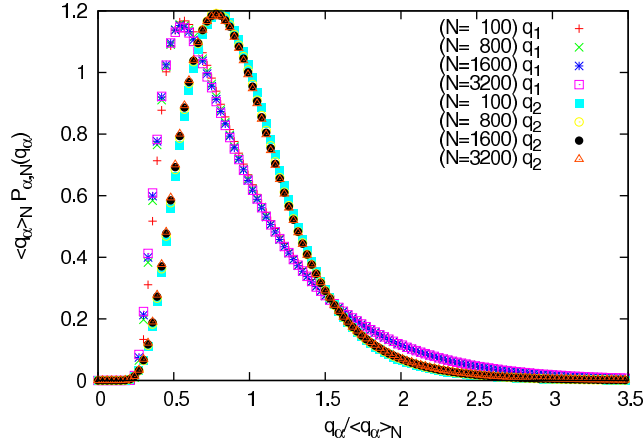


Figure 1: Rescaled distribution functions $\langle q_\alpha \rangle_N P_{\alpha,N}(q_\alpha)$ for the two eigenvalues q_α of the gyration tensor.

(3.3). The still present tiny discrepancies indicate that corrections to scaling and/or crossover effects are relevant and give rise to systematic deviations, which are larger than the statistical errors. This is consistent with the results of Ref. [17] which found $\phi = 0.435(6)$ with significant scaling corrections. Other recent estimates of ϕ are $\phi = 0.419(3)$ [20], $\phi = 0.436(7)$ (in a model with explicit solvent) [21], and $\phi = 0.422(12)$ from the analysis of the partition-function zeroes [22].

Finally, we consider the invariant ratios A_N , B_N , C_N , and F_N . MC estimates at $\beta = 0.665$ are reported in Table 2. If we exclude that data with $N = 100$, they are constant within error bars, indicating that scaling corrections and crossover effects are smaller than the statistical errors. Conservatively, we estimate the asymptotic value by averaging the results with $N \geq 1600$. We obtain

$$A_\infty = 0.18151(10) \quad (3.6)$$

$$B_\infty = 0.51106(31) \quad (3.7)$$

$$C_\infty = 0.35516(17) \quad (3.8)$$

$$F_\infty = -0.0003(7). \quad (3.9)$$

The ratios A_∞ and B_∞ are in good agreement with the results of Ref. [16]: $A_\infty = 0.180(1)$, $B_\infty = 0.510(2)$. The estimate of F_∞ is fully compatible with zero, providing further support to the conjecture $F_\infty = 0$ of Ref. [16].

4 Gyration tensor and asphericity

It has been known for many years that polymers are not instantaneously spherical in shape [29]. In order to characterize the shape we consider the gyration tensor defined

N	$\langle q_1 \rangle_N$	$\langle q_2 \rangle_N$	s_1	\mathcal{A}
100	35.543(8)	7.8954(8)	0.8182(2)	0.37668(8)
800	386.85(30)	85.871(34)	0.8183(8)	0.37569(28)
1600	859.93(37)	190.262(41)	0.8188(5)	0.37653(16)
3200	1916.6(1.5)	422.06(17)	0.8195(8)	0.37805(28)

Table 4: MC estimates of the eigenvalues of the gyration tensor, of the shape factor s_1 , and of the mean asphericity.

by

$$Q_{N,\alpha\beta} \equiv \frac{1}{2(N+1)^2} \sum_{i,j=0}^N (\omega_{i,\alpha} - \omega_{j,\alpha})(\omega_{i,\beta} - \omega_{j,\beta}), \quad (4.1)$$

which is such that $\text{Tr } Q_N = R_g^2$. The tensor $Q_{N,\alpha\beta}$ is symmetric and positive definite, hence it has two positive eigenvalues $q_1 \geq q_2$. For $N \rightarrow \infty$ they are expected to scale as

$$\langle q_\alpha \rangle_N \approx B_\alpha N^{2\nu_\theta}, \quad (4.2)$$

and to obey a scaling law of the form

$$P_{\alpha,N}(q_\alpha) = \frac{1}{\langle q_\alpha \rangle_N} F_\alpha \left(\frac{q_\alpha}{\langle q_\alpha \rangle_N} \right). \quad (4.3)$$

In Fig. 1 we report the rescaled eigenvalue distributions. All points fall quite nicely onto two different universal curves, confirming the validity of the scaling form (4.3). Note that, although the average eigenvalues differ approximately by a factor of 4.5, see Table 4, the two distribution functions are similar. They have a sharp peak for $q_\alpha/\langle q_\alpha \rangle_N \approx 0.55$ ($\alpha = 1$) and 0.75 ($\alpha = 2$), a long tail, and go to zero sharply for $q_\alpha/\langle q_\alpha \rangle_N \approx 0.25$.

To characterize quantitatively the shape of θ walks we introduce the shape factors

$$s_1 \equiv \frac{\langle q_1 \rangle_N}{\langle R_g^2 \rangle_N}, \quad s_2 \equiv \frac{\langle q_2 \rangle_N}{\langle R_g^2 \rangle_N} = 1 - s_1, \quad r_{12} \equiv \frac{\langle q_1 \rangle_N}{\langle q_2 \rangle_N} = \frac{s_1}{1 - s_1}, \quad (4.4)$$

and the mean asphericity

$$\mathcal{A} \equiv \frac{1}{2} \sum_\alpha \left\langle \frac{(q_\alpha - \bar{q})^2}{\bar{q}^2} \right\rangle_N = \left\langle \frac{(q_1 - q_2)^2}{(q_1 + q_2)^2} \right\rangle_N, \quad (4.5)$$

where $\bar{q} = \sum_\alpha q_\alpha/2 = R_g^2/2$. For a disk we have $s_1 = 1/2$, $\mathcal{A} = 0$, while a rod gives $s_1 = 1$, $\mathcal{A} = 1$.

At variance with the ratios A_N, \dots , the quantities s_1 and \mathcal{A} at $\beta = 0.665$ show a systematic drift with N , which may be an indication of the crossover towards the

asymptotic good-solvent value. To take it into account, we use the expected scaling behavior close to the θ point:

$$s_1, \mathcal{A} = f[(\beta - \beta_\theta)N^\phi]. \quad (4.6)$$

Expanding the function $f(x)$ to first order we obtain

$$s_1, \mathcal{A} = a_1 + a_2(\beta - \beta_\theta)N^\phi. \quad (4.7)$$

This implies that we should fit our data to $a_1 + bN^\phi$. The parameter a_1 gives the θ -point estimate of the universal ratio. Using $\phi = 3/7$, we obtain $s_1 = 0.8179(4)$ if we fit all data, and $s_1 = 0.8169(20)$ if we discard $N = 100$. Conservatively, we quote as final result

$$s_1 = 0.817(2). \quad (4.8)$$

From s_1 we can compute the ratio of the average eigenvalues:

$$r_{12} = 4.46(6) \quad (4.9)$$

Note that the walks are elliptical, with the major axis being approximately a factor of two longer than the minor one.

The N dependence of the average asphericity is not monotonic, and thus the fitting form (4.7) cannot describe the data up to $N = 100$. We thus only fit the data satisfying $N \geq 800$, obtaining

$$\mathcal{A} = 0.3726(7). \quad (4.10)$$

Note that the error is purely statistical and thus it does not include the systematic uncertainty due to the scaling corrections. It is interesting to compare the results for the asphericity with those obtained under good-solvent conditions [45, 46]:

$$\mathcal{A}_{\text{GS}} = 0.503(1). \quad (4.11)$$

Clearly, at the θ -point walks are more symmetric than in the good-solvent regime. Note that our result is closer to the random-walk value [47]

$$\mathcal{A}_{\text{RW}} = \frac{5}{2} - \frac{7}{4}\zeta(3) \approx 0.3964. \quad (4.12)$$

Thus, also in two dimensions, θ point interacting SAWs can be reasonably described by random walks (in three dimensions interacting SAWs are effectively random walks in the limit $N \rightarrow \infty$, although for finite N there are quite strong logarithmic corrections), as far as the shape is concerned.

5 End-to-end distribution function

5.1 Definitions

If $c_N(\mathbf{r})$ is the number of SAWs starting at the origin and ending in \mathbf{r} , we define the normalized end-to-end distribution function (EEDF) as

$$P_N(\mathbf{r}) = \frac{c_N(\mathbf{r})}{\sum_r c_N(\mathbf{r})}. \quad (5.1)$$

The mean squared end-to-end distance is related to $P_N(\mathbf{r})$ by

$$\langle R_e^2 \rangle_N = \sum_{\mathbf{r}} |\mathbf{r}|^2 P_N(\mathbf{r}). \quad (5.2)$$

In most of the studies of the EEDF one usually defines a correlation length ξ which is trivially related to R_e :

$$\xi^2 = \frac{1}{4} \langle R_e^2 \rangle_N. \quad (5.3)$$

In the following we shall always use ξ to characterize the polymer size. In the limit $N \rightarrow \infty$, $|\mathbf{r}| \rightarrow \infty$, with $|\mathbf{r}|N^{-\nu}$ fixed, the function $P_N(\mathbf{r})$ has the scaling form [33, 35, 37]

$$P_N(\mathbf{r}) \approx \frac{1}{\xi^2} f(\rho) [1 + O(N^{-\Delta})], \quad (5.4)$$

where $\boldsymbol{\rho} = \mathbf{r}/\xi$, $\rho = |\boldsymbol{\rho}|$, and Δ is a correction-to-scaling exponent. By definition

$$\int_0^\infty 2\pi\rho d\rho f(\rho) = 1, \quad (5.5)$$

$$\int_0^\infty 2\pi\rho^3 d\rho f(\rho) = 4. \quad (5.6)$$

Several facts are known about $f(\rho)$. For large values of ρ it behaves as [32, 33, 35, 37]

$$f(\rho) \approx f_\infty \rho^\sigma \exp(-D\rho^\delta), \quad (5.7)$$

where σ and δ are given by

$$\delta = \frac{1}{1 - \nu_\theta} = \frac{7}{3} \approx 2.33, \quad (5.8)$$

$$\sigma = \frac{4\nu_\theta - 2\gamma_\theta}{2(1 - \nu_\theta)} = 0. \quad (5.9)$$

For $\rho \rightarrow 0$, we have [35, 37] instead

$$f(\rho) \approx f_0 \rho^\theta, \quad (5.10)$$

where

$$\theta = \frac{\gamma_\theta - 1}{\nu_\theta} = \frac{1}{4}. \quad (5.11)$$

For the purpose of computing D and δ from Monte Carlo data, it is much easier to consider the “wall-wall” distribution function

$$P_{w,N}(x) = \sum_y P_N(x, y), \quad (5.12)$$

which represents the probability that the endpoint of the walk lies on a plane at a distance x from the origin of the walk. In the large- N limit, $P_{w,N}(x)$ has the scaling form

$$P_{w,N}(x) = \frac{1}{\xi} f_w(\rho) [1 + O(N^{-\Delta})] \quad \rho = \frac{|x|}{\xi}. \quad (5.13)$$

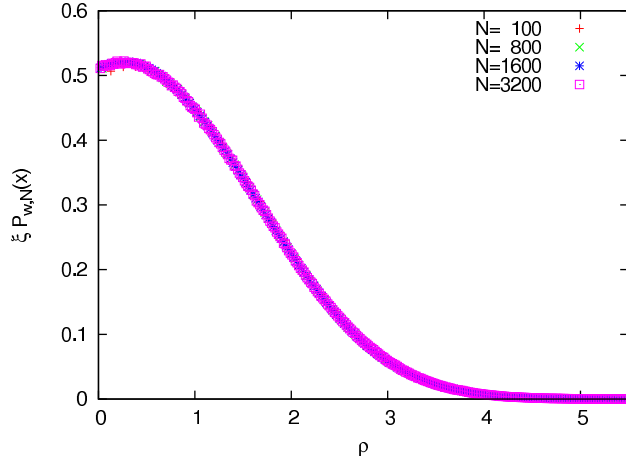


Figure 2: The wall-wall EEDF: rescaled combination $\xi P_{w,N}(x)$ vs. ρ for different values of N .

For large ρ we have

$$f_w(\rho) \approx f_{w,\infty} \rho^{\sigma_w} \exp(-D\rho^\delta), \quad (5.14)$$

where δ is given by (5.8), D is the same constant appearing in Eq. (5.7), and [44]

$$\sigma_w = \delta \left(\nu_\theta - \gamma_\theta + \frac{1}{2} \right) = -\frac{1}{6}. \quad (5.15)$$

5.2 Monte Carlo study

We studied the EEDF following closely the strategy employed in Ref. [44] to analyze the same quantity for three-dimensional non-interacting SAWs. Since our runs were performed at $\beta = 0.665 < \beta_\theta$, in principle we should reweight the MC data to obtain the EEDF at the θ -point. This correction is apparently negligible compared to the statistical errors, so that we directly analyze the results for $\beta = 0.665$ without additional corrections.

First, we consider the wall-wall distribution $P_{w,N}(x)$. In Fig. 2 we report the scaling combination $\xi P_{w,N}(x)$ versus the scaling variable ρ . The scaling is essentially perfect on the scale of the figure, confirming the correctness of Eq. (5.13). Then, we study the large- ρ behavior with the purpose of verifying the asymptotic behavior (5.14) and of determining the constants D and $f_{w,\infty}$. Our data are not precise enough to determine σ_w and thus we always fix its value in the numerical analysis. We fit the data to

$$\ln \xi P_{w,N} = \ln f_{w,\infty} - D\rho^\delta, \quad (5.16)$$

$$\ln(\rho^{1/6} \xi P_{w,N}) = \ln f_{w,\infty} - D\rho^\delta. \quad (5.17)$$

N	ρ_{\max}	ρ_{\min}	δ	D
100	4	2	2.517(3)	0.127(1)
		3	2.501(21)	0.131(5)
	5	2	2.466(6)	0.142(1)
		3	2.504(13)	0.133(3)
	6	2	2.565(14)	0.117(3)
		3	2.601(29)	0.109(6)
800	4	2	2.394(12)	0.148(3)
		3	2.410(82)	0.144(20)
	5	2	2.318(9)	0.173(3)
		3	2.305(29)	0.177(9)
	6	2	2.378(20)	0.153(6)
		3	2.361(43)	0.158(13)
1600	4	2	2.426(5)	0.141(1)
		3	2.390(30)	0.150(8)
	5	2	2.353(7)	0.164(2)
		3	2.358(21)	0.162(6)
	6	2	2.414(15)	0.144(4)
		3	2.430(32)	0.139(9)
3200	4	2	2.455(11)	0.135(2)
		3	2.423(77)	0.142(18)
	5	2	2.371(15)	0.159(4)
		3	2.375(45)	0.158(13)
	6	2	2.469(31)	0.132(8)
		3	2.493(67)	0.125(16)

Table 5: Estimates of D and δ , obtained by fitting the wall-wall EEDF to Eq. (5.16).

The two fits give correct estimates of D and δ , but only the second one provides a correct estimate of $f_{w,\infty}$. We consider only the data belonging to the range $\rho_{\min} \leq \rho \leq \rho_{\max}$. An upper cut-off ρ_{\max} is needed since scaling corrections and numerical errors increase as ρ increases. First, since $P_{w,N}(x) = 0$ for $|x| > N$, the deviations from (5.16) and (5.17) at fixed N become infinitely large as $\rho \rightarrow N/\xi \sim N^{1-\nu_\theta}$. Second, since the EEDF decreases rapidly with ρ , for ρ large there is very limited statistics, so that $P_{w,N}(x)$ has a very large error. But large- ρ data dominate in the fits, providing completely unreliable estimates of the fit parameters.

Results obtained from fits to Ansatz (5.16) are reported in Table 5, as a function of $N = 100, 800, 1600, 3200$. The results for δ do not show systematic dependences on the fit parameters ρ_{\min} and ρ_{\max} (at least in the range we consider), while they show a tiny dependence on N : apparently, for $N \geq 800$, δ increases with increasing

N	ρ_{\min}	δ	D	$\log f_{w,\infty}$
100	2	2.527(4)	0.125(1)	-0.640(5)
	3	2.545(13)	0.121(3)	-0.670(2)
800	2	2.377(10)	0.153(3)	-0.577(13)
	3	2.345(30)	0.162(9)	-0.520(53)
1600	2	2.412(7)	0.145(2)	-0.607(9)
	3	2.397(22)	0.149(6)	-0.581(37)
3200	2	2.431(15)	0.140(4)	-0.620(18)
	3	2.417(46)	0.144(12)	-0.598(78)

Table 6: Estimates of D and δ , obtained by fitting the wall-wall EEDF to Eq. (5.17) with $\rho_{\max} = 5$.

N . The reason is not fully clear but it may be again an effect of the crossover towards the good-solvent value $\delta = 1/(1 - \nu) = 4$. In any case, the results are reasonably consistent with the theoretical prediction $\delta = 7/3 \approx 2.333$. The constant D varies roughly between 0.13 and 0.17 for $N \geq 800$, so that we can estimate $D = 0.15(2)$.

In order to estimate $f_{w,\infty}$, we cannot neglect the multiplicative factor ρ^{σ_w} and thus only the results of the second fit are relevant. From the data at $N = 1600$ we obtain

$$\log f_{w,\infty} = -0.60(5), \quad f_{w,\infty} = 0.55(3), \quad (5.18)$$

where the error takes into account the estimates obtained by using all values of N .

Let us consider now the radial distribution $P_N(\mathbf{r})$. Such a quantity is not well suited for a numerical determination of the scaling function $f(\rho)$, because of fluctuations due to the lattice structure. In order to average them out, we will employ a procedure already used in this context in Refs. [40, 41, 44].

We shall consider two different averages

$$\hat{P}_{1,N}^{(\text{av})}(r_{1,n}) = \frac{1}{2N_{1,n}(r_{1,n})} \sum_{\vec{r}: r_{1,n-1}^2 < r^2 \leq r_{1,n}^2} P_N(\mathbf{r}), \quad (5.19)$$

$$\hat{P}_{2,N}^{(\text{av})}(r_{2,n}) = \frac{1}{2N_{2,n}(r_{2,n})} \sum_{\vec{r}: r_{2,n-1}^2 < r^2 \leq r_{2,n}^2} P_N(\mathbf{r}). \quad (5.20)$$

Here $r_{1,n} = r_0 + n\Delta$ and $r_{2,n}^2 = r_0^2 + n\Delta$, where r_0 and Δ are fixed parameters,¹ and $N_{1,n}(r_{1,n})$ and $N_{2,n}(r_{2,n})$ are the number of lattice points with the same parity² of N that lie in the considered shell. For practical purposes, we measure Δ in units of the

¹ Procedure (5.19) corresponds to fixing the width of the annuli on which the average is computed, while (5.20) corresponds to fixing the area (hence the number of points).

²A point (x, y) is odd (resp. even) if $x + y$ is odd (resp. even).

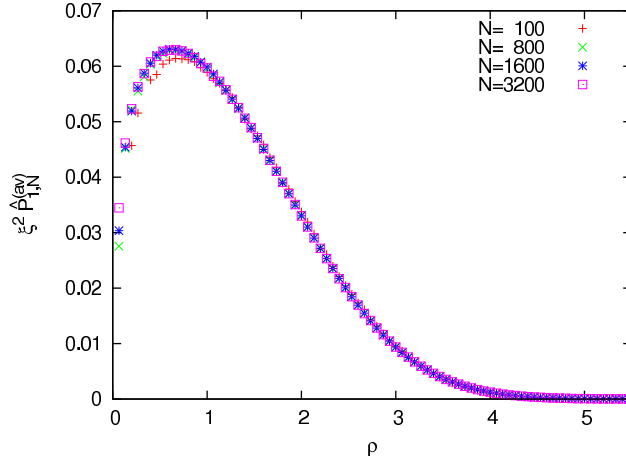


Figure 3: Rescaled EEDF $\xi^2 \hat{P}_{1,N}^{(av)}$ with $\Lambda = 1/15$ vs. ρ .

correlation length: we define $\Lambda = \Delta/\xi$ and keep it fixed for all values of N . For Δ fixed, $P_N(\mathbf{r})$, $\hat{P}_{1,N}^{(av)}(r)$, and $\hat{P}_{2,N}^{(av)}(r)$ have the same scaling behavior as $N \rightarrow \infty$. The same holds for fixed Λ , as long as $\Lambda \ll 1$. In Fig. 3 we report the rescaled EEDF obtained by using the average (5.19) with $\Lambda = 1/15$. All points fall on top of each other, except those with $N = 100$ (this is particularly evident for $\rho \lesssim 1.5$). This confirms the validity of the scaling relation (5.4).

Let us now again consider the large- ρ behavior. In order to determine the parameters, we perform fits of the form

$$\log[\xi^2 \hat{P}^{(av)}] = \log f_\infty - D\rho^\delta \quad (5.21)$$

for each N and for several ρ_{\min} , ρ_{\max} , and Λ . Note that in this case theory predicts $\sigma = 0$ and thus this fit allows us to determine f_∞ , too.

Results for $N \geq 800$, $\Lambda = 1/15$ and the fixed-width average (5.19) are reported in Table 7. The results for δ are fully consistent with the theoretical value, while those for D give roughly $D = 0.16(2)$, which is in agreement with the estimate obtained by using the wall-wall EEDF. Estimates using $\Lambda = 1/5$, or obtained by using the average (5.20) give similar results. As for f_∞ we estimate $\log f_\infty = -2.60(15)$ and $f_\infty = 0.082(11)$.

More precise estimates of D , f_∞ , and $f_{w,\infty}$ are obtained by fixing δ to its theoretical value $\delta = 7/3$. From the analysis of the wall-wall EEDF, using the fit function (5.17), we obtain

$$D = 0.1668(3) \quad f_{w,\infty} = 0.625(4), \quad (5.22)$$

while from the radial distribution function we have

$$D = 0.1656(3) \quad f_\infty = 0.088(2). \quad (5.23)$$

N	ρ_{\min}	δ	D	$\log f_{\infty}$
800	2	2.355(32)	0.158(10)	-2.566(75)
	2.5	2.340(42)	0.163(14)	-2.52(11)
	3	2.323(56)	0.170(20)	-2.46(17)
	3.5	2.296(83)	0.180(32)	-2.35(30)
1600	2	2.381(13)	0.150(4)	-2.610(32)
	2.5	2.375(17)	0.153(5)	-2.588(47)
	3	2.366(22)	0.155(7)	-2.558(70)
	3.5	2.351(32)	0.161(11)	-2.50(11)
3200	2	2.368(35)	0.154(11)	-2.589(80)
	2.5	2.355(47)	0.159(15)	-2.55(12)
	3	2.340(63)	0.164(21)	-2.50(19)
	3.5	2.317(95)	0.172(34)	-2.42(32)

Table 7: Fit results for the large-distance behavior of the radial EEDF obtained with the fixed-width average (5.19). Here $\rho_{\max} = 7$, $\Lambda = 1/15$.

The estimates of D obtained in the two cases differ by two combined error bars, indicating that the errors are underestimated by a factor of at least two. Multiplying all errors by two, we end up with the final estimates

$$D = 0.1662(6) \quad f_{w,\infty} = 0.625(8), \quad f_{\infty} = 0.088(4). \quad (5.24)$$

We finally consider the behavior for $\rho \rightarrow 0$, performing fits of the form

$$\log f(\rho) = \log f_0 + \theta \log \rho, \quad (5.25)$$

see Eq. (5.10). Since Eq. (5.25) is valid only for $\rho \rightarrow 0$ and for $r \rightarrow \infty$ (scaling limit) data must be analyzed in a window $\rho_{\min} \leq \rho \leq \rho_{\max}$. We find stable results only for $N = 3200$. For lower values of N lattice effects are very strong and Eq. (5.25) does not describe the low- r data. If we write $\rho_{\min} = n_{\min} \Lambda \xi$, we find stable results for $n_{\min} \gtrsim 1$, $0.15 \lesssim \rho_{\max} \lesssim 0.30$, and Λ quite small, $\Lambda \approx 10^{-2}$. If the parameters are in this range we obtain

$$\theta = 0.255(10), \quad (5.26)$$

$$f_0 = 0.081(2). \quad (5.27)$$

The result for θ is in perfect agreement with the theoretical prediction $\theta = 1/4$. An improved estimate of f_0 can be obtained by fixing θ to its theoretical value. We obtain

$$f_0 = 0.0810(5). \quad (5.28)$$

N	$M_{4,N}$	$M_{6,N}$	$M_{8,N}$	$M_{10,N}$	$M_{12,N}$
100	1.778(1)	4.422(4)	13.89(2)	52.2(1)	226.8(6)
800	1.815(4)	4.66(1)	15.31(7)	60.8(4)	281(3)
1600	1.819(2)	4.69(1)	15.49(4)	61.8(2)	288(2)
3200	1.818(4)	4.68(2)	15.40(7)	61.2(4)	283(3)
$N \rightarrow \infty$	1.821(4)	4.70(3)	15.5(2)	62(1)	290(10)

Table 8: The non-trivial even moments $M_{2k,N}$, $k \leq 6$, and the corresponding asymptotic values.

Finally, we computed the moments

$$M_{2k,N} = \frac{\sum_{\mathbf{r}} r^{2k} P_N(\mathbf{r})}{[\sum_{\mathbf{r}} r^2 P_N(\mathbf{r})]^k}, \quad (5.29)$$

see Table 8. We extrapolated the results by performing a fit of the form

$$M_{2k,N} = M_{2k,\infty} + aN^{-\Delta} \quad (5.30)$$

where $M_{2k,\infty}$, a , and Δ are free parameters. The results are reported in Table 8.

5.3 Phenomenological expressions

A phenomenological representation for the function $f(\rho)$ has been proposed by McKenzie and Moore [35] and des Cloizeaux [7]:

$$f(\rho) \approx f_{\text{ph}}(\rho) = f_{\text{ph}} \rho^{\theta_{\text{ph}}} \exp(-D_{\text{ph}} \rho^{\delta_{\text{ph}}}). \quad (5.31)$$

Here δ_{ph} and θ_{ph} are free parameters, while f_{ph} and D_{ph} are fixed by the normalization conditions (5.5) and (5.6):

$$\begin{aligned} D_{\text{ph}} &= \left\{ \frac{\Gamma[(4 + \theta_{\text{ph}})/\delta_{\text{ph}}]}{4 \Gamma[(2 + \theta_{\text{ph}})/\delta_{\text{ph}}]} \right\}^{\delta_{\text{ph}}/2}, \\ f_{\text{ph}} &= \frac{\delta_{\text{ph}} D_{\text{ph}}^{(2+\theta_{\text{ph}})/\delta_{\text{ph}}}}{2\pi \Gamma[(2 + \theta_{\text{ph}})/\delta_{\text{ph}}]}. \end{aligned} \quad (5.32)$$

In three dimensions in the good-solvent regime this expression describes the EEDF quite accurately, even taking δ and ρ equal to their theoretical value [44].

In our case, if we use $\theta_{\text{ph}} = \theta = 1/4$ and $\delta_{\text{ph}} = \delta = 7/3$ we obtain for the two constants

$$D_{\text{ph}} = 0.1794, \quad f_{\text{ph}} = 0.06931, \quad (5.33)$$

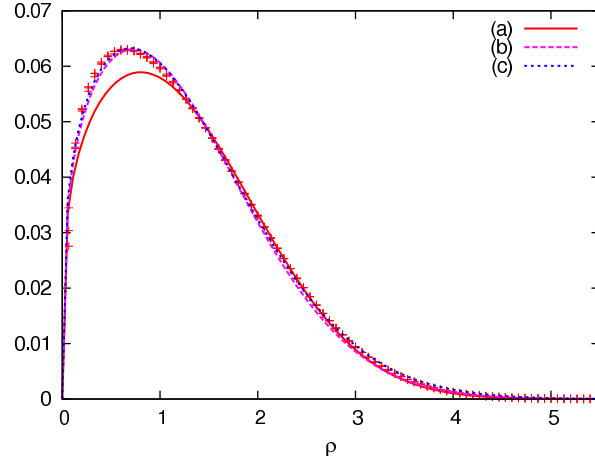


Figure 4: The EEDF against several phenomenological approximations: (a) we set $\delta_{\text{ph}} = 7/3$ and $\theta_{\text{ph}} = 1/4$ and use Eq. (5.32) to fix the constants; (b) δ_{ph} and θ_{ph} are determined by fitting the data, while the constants are fixed by Eq. (5.32); (c) δ_{ph} , θ_{ph} , D_{ph} , and f_{ph} are obtained by fitting the data.

which are quite close to the exact results. The resulting curve, curve (a) in Fig. 4, reasonably describes the EEDF in the large- and small-distance region, but underestimates it in the intermediate region $0.2 \lesssim \rho \lesssim 1.4$. As an additional check we can compute the invariant ratios M_{2k} . Using the phenomenological expression we obtain $M_{2k,\text{ph}} = 1.77, 4.39, 13.9, 53.1, 237$ for $k = 2, 3, 4, 5, 6$. They are not very much different from the exact results reported in Table 8, the differences varying between 3% for $k = 2$ and 18% for $k = 6$. Note that discrepancies increase as k increases. This is due to the fact that these ratios are increasingly sensitive to the large- ρ behavior, and the phenomenological expression underestimates the EEDF for large ρ since $D_{\text{ph}} > D = 0.1662(6)$.

In order to obtain a better approximation, we take θ_{ph} and δ_{ph} as free parameters, fixing always D_{ph} and f_{ph} by using the normalization conditions (5.32). We obtain

$$\theta_{\text{ph}} \approx 0.282, \quad \delta_{\text{ph}} \approx 2.04. \quad (5.34)$$

Correspondingly $D_{\text{ph}} = 0.270$, $f_{\text{ph}} = 0.0795$. The resulting phenomenological expression describes better the EEDF in the relevant region $\rho \lesssim 5$, see Fig. 4, but clearly overestimates the EEDF in the large- ρ region, given that δ_{ph} is smaller than $\delta = 7/3 = 2.333$. As a check we again computed the ratios M_{2k} . For $k = 2$ we obtain $M_{4,\text{ph}} = 1.825$ which agrees with the correct value $M_4 = 1.821(4)$ and confirms the validity of the approximation for ρ not too large. However, for $k \geq 3$ the obtained estimates $M_{2k,\text{ph}}$ are larger than the those reported in Table 8. For instance we obtain $M_{6,\text{ph}} = 4.96$ and $M_{8,\text{ph}} = 17.65$, which overestimate the correct results by 5% and 14%, respectively.

We obtain a slightly better approximation if we keep all constants as free parameters, relaxing the normalization conditions (5.32). We obtain

$$\theta_{\text{ph}} = 0.277, \quad \delta_{\text{ph}} = 1.95, \quad D_{\text{ph}} = 0.285, \quad f_{\text{ph}} = 0.0805. \quad (5.35)$$

The corresponding curve is reported in Fig. 4, as graph (c). It cannot be distinguished on the scale of the figure from graph (b), obtained by using parameters (5.34). This is not unexpected, since the parameters are quite close to each other. For the choice (5.35) of the constants we have

$$\int_0^\infty 2\pi\rho d\rho f(\rho) = 1.042, \quad (5.36)$$

$$\int_0^\infty 2\pi\rho^3 d\rho f(\rho) = 4.469. \quad (5.37)$$

The violations of the normalization conditions are therefore reasonably small (4% and 10% in the two cases).

5.4 Internal-point distribution function

As a byproduct of our simulations, we also determined an exponent which is related to the internal-point distribution function. We consider the probability $P_{N,M}(\mathbf{r})$ that $\omega_M - \omega_0 = \mathbf{r}$, where ω_M is an internal point, i.e. $M < N$. In the limit $N, M \rightarrow \infty$, $r \rightarrow \infty$ with $rN^{-\nu}$ and M/N fixed, we obtain the scaling expression

$$P_{N,M}(\mathbf{r}) \approx \frac{1}{\xi^2} f_{\text{int}}(r/\xi, M/N), \quad (5.38)$$

where $\xi^2 = \langle R_e^2 \rangle_N / 4$ as before. The function $f_{\text{int}}(\rho, M/N)$ is nonanalytic for $\rho \rightarrow 0$:

$$f_{\text{int}}(\rho, M/N) \sim \rho^{\theta_{\text{int}}}, \quad (5.39)$$

where the exponent θ_{int} is independent of M/N . In two dimensions θ_{int} has been computed exactly, obtaining $\theta_{\text{int}} = 5/6$ for noninteracting SAWs and $\theta_{\text{int}} = 5/12$ at the θ point [9].

The exponent θ_{int} can be determined by measuring the probability P_N^{ENN} that the endpoint is a nearest neighbor of the walk. Keeping into account that there are N internal points we obtain

$$P_N^{\text{ENN}} \sim \frac{N}{\xi^2} \xi^{-\theta_{\text{int}}} \sim N^{-2\nu - \nu\theta_{\text{int}} + 1}. \quad (5.40)$$

It should be noted that this expression only takes into account “distant” contacts, since the scaling form (5.38) is valid only in the limit $r \rightarrow \infty$. To this nonanalytic term we should therefore add the contribution of “local” contacts, which is expected to be an analytic function of N . Thus, we obtain the prediction

$$P_N^{\text{ENN}} \approx a + \frac{b}{N} + \frac{c}{N^{\nu(2+\theta_{\text{int}})-1}} + \dots \quad (5.41)$$

N	P_N^{ENN}
100	0.63307(4)
800	0.71579(10)
1600	0.73159(6)
3200	0.74407(10)

Table 9: Probability that the endpoint is a nearest neighbor of the walk.

At the θ point this gives

$$P_N^{\text{ENN}} \approx a + \frac{b}{N} + \frac{c}{N^{8/21}}, \quad (5.42)$$

while for noninteracting SAWs we have

$$P_N^{\text{ENN}} \approx a + \frac{b}{N} + \frac{c}{N^{9/8}}. \quad (5.43)$$

We have computed P_N^{ENN} at the θ point³ and fitted the results with $a + b/N^\Delta$ (see Table 9). The estimates of Δ allow us to obtain an estimate of θ_{int} :

$$\theta_{\text{int}} = 0.407(11). \quad (5.44)$$

This result is in good agreement with the theoretical value $5/12 = 0.4166\dots$. Moreover, we obtain

$$P_\infty^{\text{ENN}} = 0.7854(14). \quad (5.45)$$

6 Conclusions

In this paper we present a detailed study of some geometrical properties of two-dimensional interacting SAWs at the θ point. For this purpose we have generated walks of length up to $N = 3200$ at $\beta = 0.665$, which is close to the θ point value $\beta_\theta = 0.6673(5)$.

The main results of this investigation are the following:

- (i) We compute the critical exponents ν_θ and ϕ . Our estimate of ν_θ , $\nu_\theta = 0.570(2)$ is in perfect agreement with the Coulomb-gas prediction [9] $\nu_\theta = 4/7 \approx 0.571$. For the exponent ϕ , we find $\phi = 0.479(6)$ from the analysis of the radii, $\phi = 0.436(5)$ from the analysis of their temperature dependence, and $\phi = 0.450(4)$ from the

³We have also studied P_N^{ENN} for noninteracting SAWs in two and three dimensions. In both cases the data are well fitted by $a + b/N$, which allows us to conclude that $\theta_{\text{int}} > 2(1 - \nu)/\nu$. In two dimensions this is consistent with the theoretical prediction, while in three dimensions it implies $\theta_{\text{int}} \gtrsim 1.40$.

specific heat (errors are purely statistical). The somewhat large differences among these estimates indicate that the neglected scaling corrections are important. A reasonable final estimate would be $\phi = 0.46(3)$, which takes into account all results with their errors. Thus, we also confirm, although with limited precision, the theoretical prediction [9] $\phi = 3/7 \approx 0.429$.

- (ii) We compute several invariant ratios involving the radii R_g^2 , R_m^2 , and R_e^2 and, in particular, we verify a conjecture of Ref. [16]. For $N \rightarrow \infty$, the combination F_N defined in Eq. (2.8) vanishes, as it does for noninteracting SAWs [50, 51].
- (iii) We discuss the shape of the walks, determining, in particular, the average asphericity \mathcal{A} . We obtain

$$\mathcal{A} = 0.3726(7), \quad (6.1)$$

where the error is purely statistical. Walks are typically elliptic, the ratio of the two axes being 2.11(2). For comparison, note that for random walks [47] $\mathcal{A} = 0.3964$, while under good-solvent conditions [45, 46] $\mathcal{A} = 0.503(1)$.

- (iv) We compute the EEDF. We verify the theoretical predictions for its small- and large-distance behavior and provide effective approximations valid in the whole relevant range $r/\xi \lesssim 5$, that is for $r/\langle R_e \rangle_N \lesssim 2.5$ (for $r \gtrsim 5\xi$ the EEDF is very small).

Acknowledgements

M. Papinutto acknowledges financial support by a Marie Curie European Reintegration Grant of the 7th European Community Framework Programme under contract number PERG05-GA-2009-249309.

References

- [1] P. G. de Gennes, Phys. Lett. **38A**, 339 (1972).
- [2] M. Daoud, J. P. Cotton, B. Farnoux, G. Jannink, G. Sarma, H. Benoit, R. Du-plessix, C. Picot and P. G. de Gennes, Macromolecules **8**, 804 (1975).
- [3] J. des Cloizeaux, J. Phys. (France) **36**, 281 (1975).
- [4] V. J. Emery, Phys. Rev. **B11**, 239 (1975).
- [5] P. G. de Gennes, *Scaling Concepts in Polymer Physics* (Cornell University Press, Ithaca, NY, 1979).
- [6] K. F. Freed, *Renormalization Group Theory of Macromolecules* (Wiley, New York, 1987).

- [7] J. des Cloizeaux and G. Jannink, *Les Polymères en Solution* (Les Editions de Physique, Les Ulis, 1987); English translation: *Polymers in Solution: Their Modeling and Structure* (Oxford Univ. Press, Oxford–New York, 1990).
- [8] L. Schäfer, *Excluded Volume Effects in Polymer Solutions* (Springer Verlag, Berlin, 1999).
- [9] B. Duplantier and H. Saleur, Phys. Rev. Lett. **59**, 539 (1987).
- [10] T. Ishinabe, J. Phys. A **20**, 6435 (1987).
- [11] F. Seno and A. L. Stella, J. Physique (France) **49**, 739 (1988).
- [12] D. Maes and C. Vanderzande, Phys. Rev. A **41**, 3074 (1990).
- [13] H. Meirovitch and H. A. Lim, J. Chem. Phys. **92**, 5144 (1990).
- [14] D. P. Foster, E. Orlandini, and M. C. Tesi, J. Phys. A **25**, L1211 (1992).
- [15] I. Chang and H. Meirovitch, Phys. Rev. E **48**, 3656 (1993).
- [16] A. L. Owczarek, T. Prellberg, D. Bennett-Wood, and A. J. Guttmann, J. Phys. A **27**, L919 (1994).
- [17] P. Grassberger and R. Hegger, J. Physique (France) I **5**, 597 (1995).
- [18] P. P. Nidras, J. Phys. A **29**, 7929 (1996).
- [19] D. Bennett-Wood, I. G. Enting, D. S. Gaunt, A. J. Guttmann, J. L. Leask, A. L. Owczarek, and S. G. Whittington, J. Phys. A: Math. Gen. **31**, 4725 (1998).
- [20] S. L. Narasimhan, P. S. R. Krishna, K. P. N. Murthy, and M. Ramanadham, Phys. Rev. E **65**, 010801(R) (2001).
- [21] M. Gaudreault and J. Viñals, Phys. Rev. E **80**, 021916 (2009).
- [22] J. H. Lee, S.Y. Kim, and J. Lee, J. Chem. Phys. **133**, 114106 (2010).
- [23] A. L. Owczarek, T. Prellberg, and R. Brak, Phys. Rev. Lett. **71**, 4275 (1993).
- [24] A. L. Owczarek, J. Phys. A: Math. Gen. **26**, L647 (1993).
- [25] P. Grassberger and H.-P. Hsu, Phys. Rev. E **65**, 031807 (2002).
- [26] H.-P. Hsu and P. Grassberger, J. Phys. A: Math. Gen. **35**, L759 (2002).
- [27] M. Baiesi, E. Orlandini, and A. L. Stella, Phys. Rev. Lett. **96**, 040602 (2006).
- [28] A. L. Owczarek and T. Prellberg, Phys. Rev. E **67**, 032801 (2003).
- [29] W. Kuhn, Kolloid Z. **68**, 2 (1934).

- [30] H. A. Kramers, J. Chem. Phys. **14**, 415 (1946).
- [31] F. H. Abernathy, J. R. Bertschy, R. W. Chin, D. E. Keyes, J. Rheol. **24**, 647 (1980).
- [32] M. E. Fisher and B. J. Hiley, J. Chem. Phys. **34**, 1253 (1961).
- [33] M. E. Fisher, J. Chem. Phys. **44**, 616 (1966).
- [34] J. Mazur, J. Res. Natl. Bur. Stand. **A69**, 355 (1965); J. Chem. Phys. **43**, 4354 (1965).
- [35] D. S. Mc Kenzie and M. A. Moore, J. Phys. **A4**, L82 (1971).
- [36] D. S. Mc Kenzie, Phys. Rep. **27C**, 35 (1976).
- [37] J. des Cloizeaux, Phys. Rev. **A10**, 1665 (1974); J. Physique **41**, 223 (1980).
- [38] M. Bishop and J. H. R. Clarke, J. Chem. Phys. **94**, 3936 (1991).
- [39] M. Bishop, J. H. R. Clarke, A. Rey, and J. J. Freire, J. Chem. Phys. **95**, 4589 (1991).
- [40] J. Dayantis and J.-F. Palierne, J. Chem. Phys. **95**, 6088 (1991).
- [41] N. Eizenberg and J. Klafter, J. Chem. Phys. **99**, 3976 (1993).
- [42] J. S. Pedersen, M. Laso, and P. Schurtenberger, Phys. Rev. **E54**, R5917 (1996).
- [43] J. P. Valleau, J. Chem. Phys. **104**, 3071 (1996).
- [44] S. Caracciolo, M. S. Causo, and A. Pelissetto, J. Chem. Phys. **112**, 7693 (2000).
- [45] M. Bishop, J. H. R. Clarke, A. Rey, and J. J. Freire, J. Chem. Phys. **95**, 608 (1991).
- [46] C. von Ferber, J. Yates Monteith, and M. Bishop, Macromolecules **42**, 3627 (2009).
- [47] H. W. Diehl and E. Eisenriegler, J. Phys. A: Math. Gen. **22**, L87 (1989).
- [48] G. T. Barkema, U. Bastolla and P. Grassberger, J. Stat. Phys. **90**, 1311 (1998), cond-mat/9707312.
- [49] A. G. Cunha-Netto, R. Dickman, and A. A. Caparica, Comp. Phys. Comm. **180**, 583 (2009).
- [50] S. Caracciolo, A. Pelissetto, A. D. Sokal, J. Phys. A: Math. Gen. **23**, L969 (1990).
- [51] J. L. Cardy, H. Saleur, J. Phys. A: Math. Gen. **22**, L601 (1989).

- [52] S. Caracciolo, M. S. Causo, G. Ferraro, M. Papinutto, and A. Pelissetto, J. Stat. Phys. **100**, 1111 (2000).
- [53] S. Caracciolo, M. Papinutto, and A. Pelissetto, Phys. Rev. E **65**, 031106 (2002).

